Giant Nernst Effect and Bipolarity in the Quasi-One-Dimensional Metal $Li_{0.9}Mo_6O_{17}$

J. L. Cohn,[1] B. D. White,[2] C. A. M. dos Santos,[3] and J. J. Neumeier[2]

[1]*Department of Physics, University of Miami, Coral Gables, Florida 33124, USA*
[2]*Department of Physics, Montana State University, Bozeman, Montana 59717, USA*
[3]*Escola de Engenharia de Lorena—USP, P. O. Box 116, Lorena-SP, 12602-810, Brazil*

(Received 22 September 2011; published 2 February 2012)

The Nernst coefficient for the quasi-one-dimensional metal, $Li_{0.9}Mo_6O_{17}$, is found to be among the largest known for metals ($\nu \simeq 500$ μV/KT at $T \sim 20$ K), and is enhanced in a broad range of temperature by orders of magnitude over the value expected from Boltzmann theory for carrier diffusion. A comparatively small Seebeck coefficient implies that $Li_{0.9}Mo_6O_{17}$ is bipolar with large, partial Seebeck coefficients of opposite sign. A very large thermomagnetic figure of merit, $ZT \sim 0.5$, is found at high field in the range $T \approx 35$–50 K.

DOI: 10.1103/PhysRevLett.108.056604 PACS numbers: 72.15.Eb, 72.15.Gd, 72.15.Jf

The Nernst effect, a transverse electric field generated by a longitudinal temperature gradient in the presence of a perpendicular magnetic field, has been known since its discovery in the 19th century in the semimetal bismuth [1]. Conductors with large Nernst coefficients are potential candidates for use in cryogenic refrigeration [2], but in spite of several decades' research and a demand for such devices at temperatures below 100 K (e.g., for infrared detectors), none have yet proved practical. In recent years, Nernst-effect measurements have received renewed attention as a means for probing the pseudogap phase of cuprate superconductors [3,4] and novel ground states of other correlated-electron systems [5], prompting a reassessment of the physics leading to large Nernst coefficients in metals. Emphasizing the contribution from diffusing charge carriers, experiment and theory agree [5] that the Nernst-coefficient magnitude is set by the ratio of charge-carrier mobility to Fermi energy. Here we report observations of very large Nernst coefficients in the quasi-one-dimensional (Q1D) metal, $Li_{0.9}Mo_6O_{17}$, rivaling the largest known for bismuth and graphite. This material possesses neither a very large mobility nor a small Fermi energy. We establish that conduction along the Q1D chains of this material is bipolar, with very large partial thermopowers of opposite sign that predominate over conventional carrier diffusion in a broad temperature range. The observations offer new insight into the origin of large thermoelectric coefficients in bulk conductors and expand the criteria for viable materials in thermomagnetic cooling applications.

$Li_{0.9}Mo_6O_{17}$, a low-temperature superconductor ($T_c \approx 2$ K) first synthesized and studied in the 1980s [6,7], has attracted interest more recently for its quasi–one dimensionality and Luttinger-liquid candidacy [8–11]. This compound is unusual among inorganic and organic Q1D compounds in its absence of a conventional density-wave transition [12,13] (either charge or spin) throughout a broad temperature range, $T \geq T_c$. An upturn in its resistivity below $T_M \sim 30$ K may be associated with localization, dimensional crossover or the development of unconventional (e.g., electronically driven) charge density-wave order [12–14]. Though the $T \rightarrow 0$ ground state (superconducting, metallic, or insulating) is sensitive to heat treatment and can vary among as-prepared crystals [15], the anisotropy and temperature variation of electrical properties for $T \geq 5$ K, the regime of study here, are robust and reproducible [12–17].

Single-crystal growth of $Li_{0.9}Mo_6O_{17}$ is described in detail elsewhere [7,13]. Crystals had typical dimensions 0.05–0.15 mm along a and 0.5–2 mm in the b-c plane. Longitudinal and transverse voltages were measured with Au leads attached with silver epoxy. A 25 μm-diameter chromel-constantan differential thermocouple monitored the temperature difference. The Nernst signal at each field was determined from the slope of linear $V_H - \Delta T_x$ curves (with V_H the field-odd transverse voltage). Lattice constants and oxygen content for six crystals studied and additional details on the transport measurements are described in the Supplemental Material [18].

Complete sets of transport measurements (resistivity, thermopower, thermal conductivity, Hall and Nernst coefficients) were measured on two single crystals of $Li_{0.9}Mo_6O_{17}$ (LMO), designated $A2$ and C, with electric or heat currents along the Q1D Mo-O chains (crystallographic b axis; inset Fig. 1). The Nernst coefficient of specimen C was also measured with heat current along the c axis. Thermal and thermoelectric measurements (heat flow along b) were also performed on a third crystal, designated D. For heat flow along the x direction (temperature gradient, $\nabla_x T$) and magnetic field along z, the Nernst coefficient is defined as $\nu_{yx} = -E_y/(\nabla_x T B_z)$.

With magnetic field along the least conducting a axis, ν_{cb} and ν_{bc} were determined for specimens $A2$ and C and ν_{cb} for specimen D as shown in Fig. 1(a) [18]. The observed ratio, $\nu_{cb}/|\nu_{bc}| \sim 3$–6, reflects the resistivity anisotropy, ρ_c/ρ_b, and agrees well with measurements on similar crystals [16,17]. $\nu(T)$ in nonmagnetic metals may have contributions from charge-carrier diffusion and from phonon drag, the latter arising from the interaction of the

 © 2012 American Physical Society

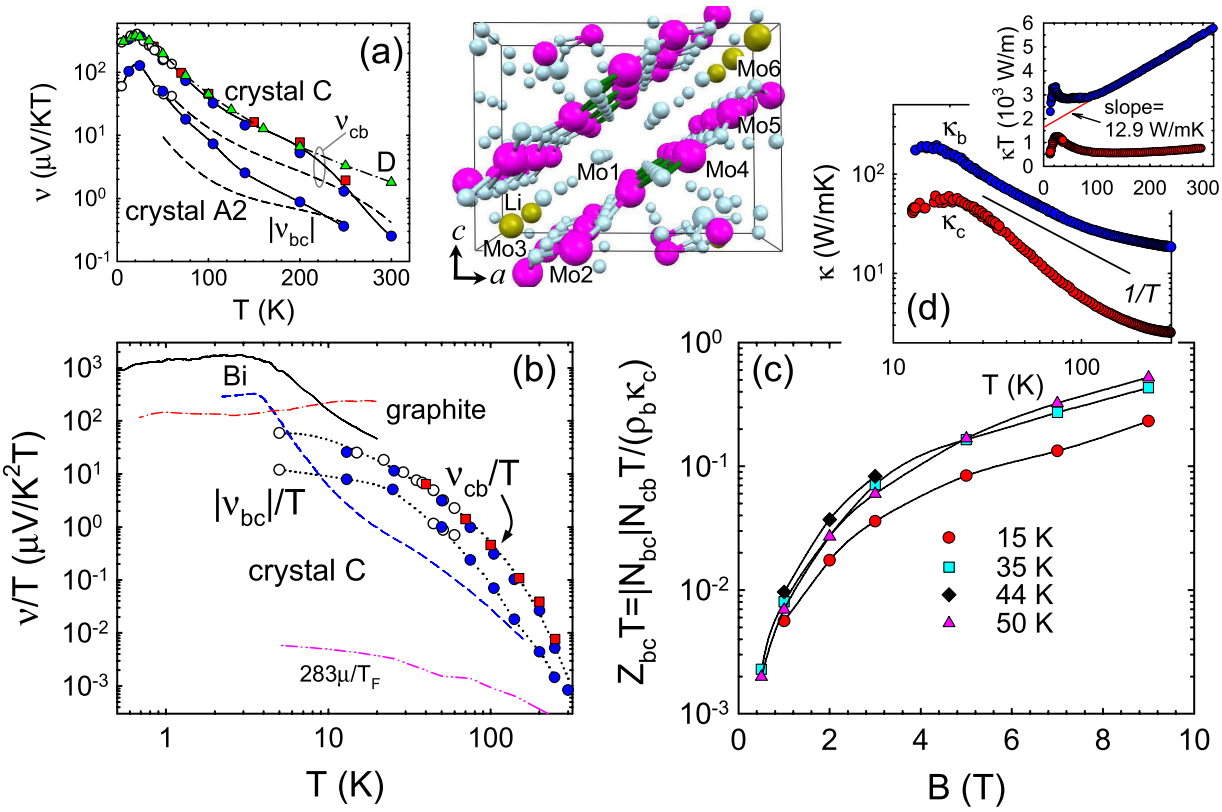

FIG. 1 (color online). (a) Nernst coefficient, $\nu(T)$, for crystals $A2$ (dashed lines), C (circles and squares), and D (triangles). For crystal C: ν_{cb} and ν_{bc} determined with primary heat current along b (solid circles) and c (solid squares), respectively. The specimen, originally with thickness 110 μm along a, was mechanically thinned to 55 μm and remeasured with primary heat current along b (open circles) [18]. (b) ν/T vs T for crystal C, compared to bismuth [Refs. [19] (solid curve) and [20] (dashed curve)] and graphite (Ref. [21]). The dash-dot-dotted curve labeled "$283\mu/T_F$" represents the carrier-diffusion contribution from Boltzmann theory, determined from the carrier mobilities and estimated Fermi temperature [18]. (c) Figure of merit as a function of magnetic field for crystal C at several temperatures. (d) zero-field thermal conductivities along the b and c axes, inset: same data plotted as κT vs T to emphasize the large constant term in $\kappa_b(T)$. Main Inset: Perspective view of the LMO monoclinic unit cell viewed along the b axis; Q1D Mo1-O-Mo4 zigzag double chains composed of MoO_6 octahedra (highlighted bonds) are part of planar Mo-O networks whose two dimensionality is broken by the Li ions.

carriers with a nonequilibrium population of heat-carrying phonons. The diffusion term can be expressed as [5,22], $\nu/T \simeq (\pi^2/3)(k_B/e)(\mu/T_F) = 283(\mu/T_F)$, where μ is the carrier mobility and T_F the Fermi temperature. This expression approximates ν/T quite well at low T (within a factor of 3–5) for Bi, graphite, and a variety of other multiband, correlated, and/or low-dimensional metals [5], over 6 orders of magnitude in μ/T_F [18]. The ν/T data for LMO [Fig. 1(b)] exceed an estimate of this diffusion contribution (dash-dot-dot curve) by 4 orders of magnitude at low T, and remain significantly larger to room temperature. The expression is strictly valid for a linear energy dependence of the Hall angle at the Fermi level. Though strong energy-dependent scattering, as may arise from electron correlations or incipient density-wave order, or proximity to a quantum critical point [5], can enhance this energy dependence and hence ν/T, it is very unlikely such effects can account for this very large discrepancy [22]. We conclude that a mechanism other than carrier diffusion predominates in $\nu(T)$ over the entire temperature range.

Consider the potential of LMO for application. For operation as an Ettingshausen cooler, with electric current applied along the b axis generating heat flow along c, the relevant adiabatic thermomagnetic figure of merit is [2], $Z_{bc}T = N_{bc}N_{cb}T/(\rho_b\kappa_c)$ where $N = \nu B$ and κ_c is the c-axis thermal conductivity. Figure 1(c) shows the field dependence of $Z_{bc}T$ along with $\kappa_c(T)$ [Fig. 1(d)]; the latter is independent of field. We see that ZT at 35 K reaches 0.5 for $B = 9$ T with no sign of saturation, among the highest known values for any material [23,24]. Viable thermomagnetic materials for applications should have ZT approaching 1 at fields achievable using small permanent magnets ($B \lesssim 1$ T). It is conceivable that the interchain κ_c can be reduced (e.g., through the introduction of mass disorder via chemical substitution) to enhance ZT at lower field.

The Seebeck coefficient or thermopower (TEP), $S = -E_x/\nabla_x T$, reveals an important aspect of conduction in LMO. Crystals C and D with the largest $\nu(T)$ have TEP values (Figs. 2 and 3) that are modest in magnitude. Consequently, the ratio of transverse to longitudinal

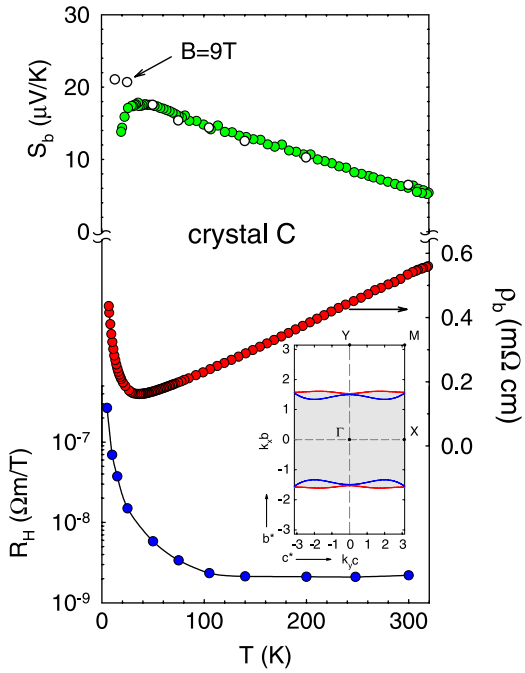

FIG. 2 (color online). Seebeck coefficient (S), resistivity, and Hall coefficient for specimen C. Inset: Fermi surface for $Li_{0.9}Mo_6O_{17}$ (adapted from Ref. [9]).

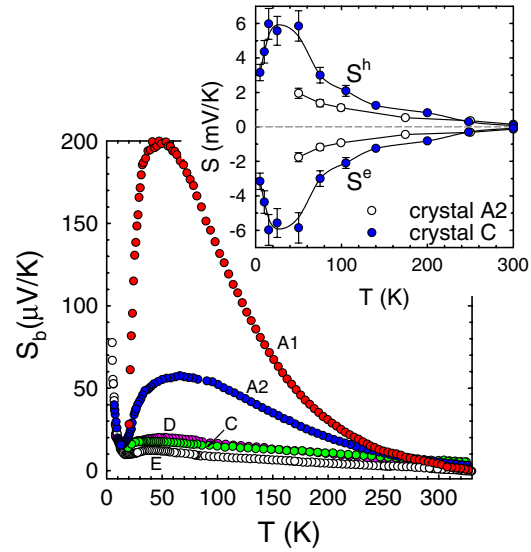

FIG. 3 (color online). Zero-field b-axis Seebeck coefficient for four $Li_{0.9}Mo_6O_{17}$ specimens. Combined results of x-ray, compositional, and Hall measurements indicate that specimens with large peaks ($A1$, $A2$) are more oxygenated and particle-hole asymmetric ($R^h \gg R^e$ and $\sigma^h < \sigma^e$) compared to those with linear-T thermopowers (C, D, E) [18]. Inset: Hole and electron partial thermopowers computed using the equation [25], the measured Nernst coefficient (ν_{cb}), and two-band model parameters; error bars (25%) are propagated from those of the Hall data [18].

thermoelectric fields, $E_y/E_x = \nu B/S$, exceeds 10^2 at 40 K; the electric field is essentially perpendicular to the temperature gradient. The implication is that LMO is compensated, with a cancellation of very large hole and electron Seebeck coefficients (opposite in sign). This can be seen more explicitly from the expression for ν in a bipolar, anisotropic conductor [25] which includes a bipolar term involving the difference, $S^h - S^e$, of the hole and electron partial Seebeck coefficients along the heat flow. For perfect compensation, $\nu_{cb} \simeq (1/2)\mu_b(S_b^h - S_b^e)$, while $S_b = (1/2)(S_b^h + S_b^e)$. Bipolarity is plausible given the band structure [8,9,26] composed of two nearly degenerate, approximately 1/2-filled, Q1D bands of Mo d_{xy} parentage crossing the Fermi energy; there are two pairs of slightly warped Fermi surface (FS) sheets in the $b^* - c^*$ planes (inset, Fig. 2). Each sheet, with positive and negative curvature, can contribute electron and hole character if the mean free path is anisotropic [27]. Bipolarity is well known to enhance the Nernst effect and is a prerequisite for useful thermomagnetic materials.

Supporting this bipolar picture, the TEP of other crystals with higher oxygen content, like $A1$ and $A2$ (Fig. 3), exhibit very large, positive maxima at $T = 50$–70 K that augment the linear-T form (specimens C, D, E) up to 300 K and beyond (previously published data for the TEP of LMO [28] fall between those of specimens $A2$ and C). This behavior and the smaller Nernst coefficient for specimen $A2$ are consistent with a departure from electron-hole symmetry in the more oxygenated crystals and incomplete cancellation of very large partial thermopowers.

A two-component analysis of the transport places these qualitative observations on a quantitative footing. Magnetoresistance and Hall data [18] for crystal C yield $R^h \simeq -R^e \simeq 3.4 \times 10^{-8}$ Ω m/T at 300 K and $\sigma^h \simeq \sigma^e$ such that the measured Hall coefficient (Fig. 2) is an order of magnitude smaller than R^h or $|R^e|$, consistent with the substantial cancellation implied by the thermoelectric coefficients. The effective carrier density $\approx 2/(R^h|e|) \simeq 3.7 \times 10^{26}$ m^{-3} represents ~13% of that estimated from the chemistry or bonding [18], suggesting localization of a significant fraction of carriers at the FS in accord with optical studies [12]. A similar analysis of transport data for crystal $A2$ [18] yields $R^h \simeq 7|R^e|$, $\sigma^h \simeq 0.4\sigma^e$, and a mobile carrier fraction ~2.5%. Using these hole and electron transport coefficients and the measured $\nu_{cb}(T)$, the equation for ν [25] can be inverted to compute $S_b^h(T)$ and $S_b^e(T)$ for the two crystals (inset, Fig. 3). In generating these curves it was assumed that $\sigma_c^h/\sigma_c = \sigma_b^h/\sigma_b$, but relaxing this assumption yields comparable TEP magnitudes [18]. The colossal TEP values (2–6 mV/K at low T) are typical of semiconductors [29], but are unprecedented for metals.

We hypothesize that the computed TEP is substantially larger than the intrinsic chain-axis value because the measured σ_b in LMO is suppressed by the occurrence of incomplete electrical connectivity of the Mo-O chains. This hypothesis is motivated by the Hall data implying a large fraction of localized carriers, and the observation of a

large constant term in $\kappa_b(T)$ (12.9 W/mK) at $T \geq 80$ K [inset, Fig. 1(d)]. The latter is attributed to electronic heat conduction. Poor connectivity will substantially suppress the measured σ_b from that of continuous chains, whereas electronic heat conduction on chain fragments will continue to contribute given that heat is transferred readily to the lattice. Supporting this picture, the constant term in κ_b varies little among several other crystals with varying σ_b [18]. This scenario is appealing because it can simultaneously account for the large fraction of total charge that is localized and the different values for the anisotropy ratio σ_b/σ_c reported in the literature [6,16,17,30]. It also favors a Sommerfeld value for the Lorenz number ($L_0 = 2.45 \times 10^{-8}$ W Ω/K^2): the resistivity for specimen C and its estimated mobile carrier fraction ($f = 0.13$) from the Hall measurement yields, $\kappa_b^e(300\text{ K}) = (L_0/f) \times 0.55 \times 10^{-5}(\Omega\text{m})^{-1} \times 300\text{ K} = 10$ W/mK. A bipolar thermal conductivity [31], expected in a metal with overlapping bands at E_F, should also contribute $\lesssim 1$ W/mK. Bipolar heat flow should dominate the thermal Hall conductivity (Righi-Leduc effect) of a closely compensated system, offering an alternative explanation for recent observations of an apparent Wiedemann-Franz law violation [30] in LMO based on such measurements. An intrinsic chain resistivity at 300 K, $\rho_{ch} = f\rho_b \simeq 70\ \mu\Omega$ cm and Hall mobility $\mu_{ch} \simeq (\mu_b/f) \simeq 2.3 \times 10^{-2}$ T^{-1} are inferred. The computed partial thermopowers (Fig. 3), depending inversely on σ_b [25], should be reduced accordingly by the factor f.

On the other hand, the measured thermoelectric coefficients reflect appropriate bulk averages, weighing voltage contributions from short and long chain fragments according to local temperature differences. Thus the intrinsic chain thermoelectric behavior must be closest to that of the most conducting specimen C, having the largest value of ν and smallest of the TEP (the most closely compensated). The deviation from particle-hole symmetry and increased carrier localization characterizing more oxygenated crystals presumably reflect the combined effects of charge doping and disorder associated with oxygen defects [15]. The electronic system of LMO is most one dimensional at high T where the thermal energy exceeds the transverse hopping energy ($t_\perp$) that determines the warping of the FS sheets [32]. This is the regime where a conventional phonon-drag mechanism is least likely to explain the large thermoelectric coefficients since anharmonic phonon-phonon scattering should limit momentum transfer to the electron system, rendering phonon drag negligible. However, it is possible the low dimensionality of the lattice [13] suppresses phonon-phonon scattering along the chains [33], thereby enhancing phonon drag in this regime. It is difficult to assess the possible relevance of Luttinger physics. Theoretical treatments of the thermopower for single Luttinger chains with impurity scattering [34] indicate a linear temperature dependence, inconsistent with the present results. More realistic models including electron-electron Umklapp scattering and coupled chains (essential for the Nernst effect) have not been treated to our knowledge. At $T \leq T_M$, where higher-dimensional behavior is manifested in unconventional density-wave order [12–14] and the appearance of superconductivity, large phonon-drag effects are plausible, particularly near $T = 20$ K where both κ_b and ν exhibit maxima (Fig. 1). There the phonon mean free path Λ is $\sim 10\ \mu$m, as inferred from kinetic theory using the measured specific heat [12] and an acoustic phonon velocity $v \simeq 3$ km/s. This implies a phonon-drag TEP [35], $S_g \simeq v\Lambda/\mu_{e\text{-}ph}T \approx 750\ \mu$V/K using $\mu_{e\text{-}ph} = 2$ T^{-1} (estimated as 5 times the average μ/f for specimen C), in good agreement with the computed partial TEP value (corrected by the factor f).

In summary, $Li_{0.9}Mo_6O_{17}$ is found to have a bipolar Nernst coefficient that is among the largest known for metals and far exceeds the expected contribution from carrier diffusion over a broad temperature range. Though phonon drag appears capable of accounting for this discrepancy at the lowest T, low-dimensional physics of the electronic and/or lattice systems may be important to a complete understanding of its enhanced thermoelectric coefficients.

The authors acknowledge very helpful input from A. L. Chernyshev. This material is based upon work supported by the National Science Foundation under Grant No. DMR-0907036 (Mont. St. Univ.), the Research Corporation (Univ. Miami), and in Lorena by the CNPq (301334/2007-2) and FAPESP (2009/14524-6).

[1] A. V. Ettingshausen and W. Nernst, Ann. Phys. (Leipzig) **265**, 343 (1886).
[2] F. Freibert, T. W. Darling, A. Migliori, and S. Trugman, Semicond. Semimet. **70**, 207 (2001).
[3] Y. Wang, L. Li, and N. P. Ong, Phys. Rev. B **73**, 024510 (2006).
[4] R. Daou *et al.*, Nature (London) **463**, 519 (2010).
[5] K. Behnia, J. Phys. Condens. Matter **21**, 113101 (2009).
[6] M. Greenblatt, Chem. Rev. **88**, 31 (1988).
[7] W. H. McCarroll and M. Greenblatt, J. Solid State Chem. **54**, 282 (1984).
[8] G.-H. Gweon *et al.*, J. Electron Spectrosc. Relat. Phenom. **117–118**, 481 (2001).
[9] Z. S. Popović and S. Satpathy, Phys. Rev. B **74**, 045117 (2006).
[10] Feng Wang *et al.*, Phys. Rev. Lett. **96**, 196403 (2006).
[11] J. Hager *et al.*, Phys. Rev. Lett. **95**, 186402 (2005).
[12] J. Choi *et al.*, Phys. Rev. B **69**, 085120 (2004).
[13] C. A. M. dos Santos *et al.*, Phys. Rev. Lett. **98**, 266405 (2007).
[14] X. Xu *et al.*, Phys. Rev. Lett. **102**, 206602 (2009).
[15] C. A. M. dos Santos *et al.*, Phys. Rev. B **77**, 193106 (2008).
[16] M. S. da Luz *et al.*, Phys. Rev. B **76**, 233105 (2007).
[17] H. Chen *et al.*, Europhys. Lett. **89**, 67010 (2010).
[18] See Supplemental Material at http://link.aps.org/supplemental/10.1103/PhysRevLett.108.056604 for measurement details, additional data, and analysis.

[19] K. Behnia, M.-A. Méasson, and Y. Kopelevich, Phys. Rev. Lett. **98**, 076603 (2007).
[20] I. Ya. Korenblit, M. E. Kuznetsov, and S. S. Shalyt, Sov. Phys. JETP **29**, 4 (1969).
[21] Z. Zhu *et al.*, Nature Phys. **6**, 26 (2009).
[22] V. Oganesyan and I. Ussishkin, Phys. Rev. B **70**, 054503 (2004).
[23] R. B. Horst and L. R. Williams, in *Proceedings of the 3rd International Conference on Thermoelectric Energy Conversion* (IEEE, New York, Arlington, TX, 1980), p. 183.
[24] A. Pourret *et al.*, Phys. Rev. Lett. **96**, 176402 (2006).
[25] The Nernst coefficient for an anisotropic, bipolar conductor can be written as [see H. J. Goldsmid, Br. J. Appl. Phys. **14**, 271 (1963)], $\nu_{yx} = (\frac{\sigma_x}{\sigma_y})\frac{\sigma_x^h \nu_{yx}^h + \sigma_x^e \nu_{yx}^e}{\sigma_x} + \frac{(R^h\sigma_y^h - R^e\sigma_y^e)\sigma_x^h\sigma_x^e(S_x^h - S_x^e)}{\sigma_x\sigma_y}$, where $R^h(R^e)$ and $S^h(S^e)$ are the hole (electron) Hall and partial Seebeck coefficients, respectively, and $\sigma_x \equiv \sigma_x^h + \sigma_x^e$, etc., for σ_y.
[26] M. H. Whangbo and E. Canadell, J. Am. Chem. Soc. **110**, 358 (1988).
[27] N. P. Ong, Phys. Rev. B **43**, 193 (1991).
[28] M. Boujida *et al.*, Physica (Amsterdam) **153C–155C**, 465 (1988).
[29] A. Bentien *et al.*, Europhys. Lett. **80**, 17 008 (2007).
[30] N. Wakeham *et al.*, Nature Commun. **2**, 396 (2011).
[31] C. F. Gallo, J. Appl. Phys. **36**, 3410 (1965).
[32] T. Giamarchi, Chem. Rev. **104**, 5037 (2004).
[33] D. T. Morelli *et al.*, Phys. Rev. Lett. **57**, 869 (1986).
[34] C. L. Kane and M. P. A. Fisher, Phys. Rev. Lett. **76**, 3192 (1996); I. A. Romanovsky *et al.*, Phys. Rev. B **65**, 075115 (2002).
[35] B. Tieke *et al.*, Phys. Rev. B **58**, 2017 (1998).

Supplementary Material

J. L. Cohn, B. D. White, C. A. M. dos Santos, and J. J. Neumeier

Properties of the crystals studied

TABLE I: Lattice constants, oxygen content as determined by energy-dispersive x-ray spectroscopy, and Hall coefficient (at 250 K) for the six $Li_{0.9}Mo_6O_{17}$ crystals studied in this paper.

Specimen	a (Å)	b (Å)	c (Å)	Wt.% O	R_H ($10^{-9}\Omega$ m/T)
A1	12.751(2)	5.521(2)	9.475(5)	32.1(3)	–
A2[a]	12.752(2)	5.520(2)	9.482(4)	–	3.3
B	12.751(2)	5.520(2)	9.486(5)	30.6(4)	–
C	12.753(2)	5.520(2)	9.491(4)	–	2.1
D	12.753(2)	5.519(2)	9.488(4)	–	–
E	12.751(2)	5.520(2)	9.489(3)	29.7(3)	–

[a]crystal A2 is the same as specimen A1, but measured 18 months later with fresh electrical contacts. The implication is that crystals tend to lose oxygen over time.

Transport measurements

For thermoelectric measurements specimens were suspended in vacuum with one end attached to a Cu cold sink (silver epoxy) and the other affixed with a small metal-film chip heater (varnish). Longitudinal and transverse voltages were measured with Au leads attached with silver epoxy. A 25 μm-diameter chromel-constantan differential thermocouple monitored the temperature difference across the sample and a separate chromel-constantan thermocouple monitored the average sample temperature (relative to the calibrated thermometer mounted in the cold sink). A high-precision, differential method was employed at fixed magnetic fields to determine the Nernst coefficient: at each field the heater current was cycled through three different values and voltages measured after a steady state was achieved. This process was repeated for reversed magnetic field. The Nernst signal at each field was determined from the slope of resulting linear V_H-ΔT_x curves, with $V_H = [V_{xy}(B) - V_{xy}(-B)]/2$ the field-odd transverse voltage (Fig. S2 a). The Nernst signal was linear in magnetic field at all temperatures for $B \lesssim 3$ T (Fig. S2 b). Nonlinearity

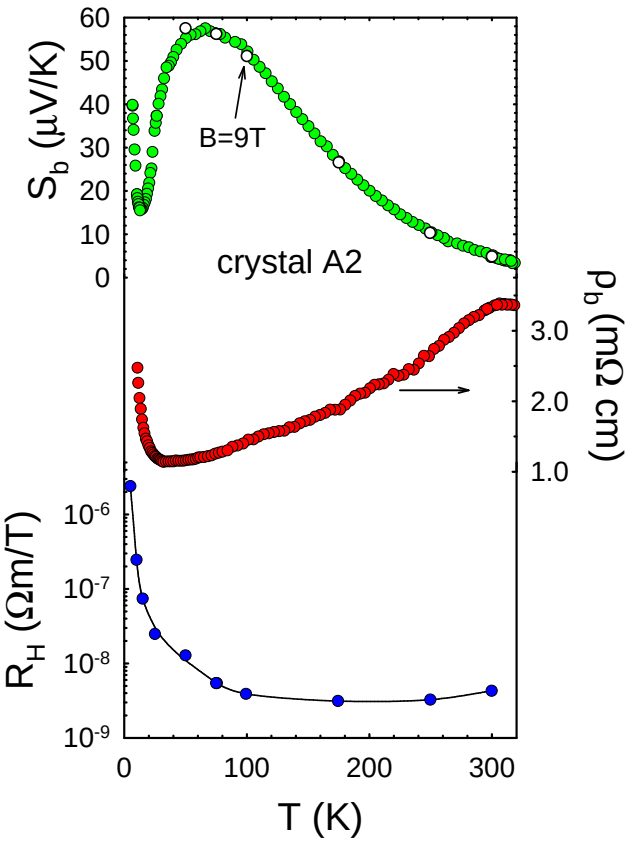

Fig. S 1: Seebeck coefficient (S), resistivity, and Hall coefficient for specimen A2 along the conducting chains.

at higher fields was evident at temperatures $T \lesssim 35$ K. The Nernst coefficient was computed from the low-field slope in these plots. The field dependence of the thermocouple[1] for temperatures $T \geq 10$ K is $\lesssim 5\%$.

The Hall coefficient was measured during the same experimental runs. Linearity of the Hall voltage in applied current and magnetic field was observed for $T \geq 50$ K. Some nonlinearity in field was observed at lower temperatures. The Hall coefficients of both specimens A2 and C were re-measured in subsequent experiments under isothermal conditions (varnished flat to the heat sink); good agreement was found with both sets of measurements.

For thermal-conductivity measurements, heat losses associated with radiation and conduction through the leads were assessed in separate experiments with specimens suspended from their leads in vacuum. The data presented in Fig. 1 d have been corrected accordingly. These corrections amounted to 30% near 300 K for κ_c and 5% for κ_b. At $T \leq 100$ K the corresponding corrections were $< 6\%$ and $< 1\%$, respectively.

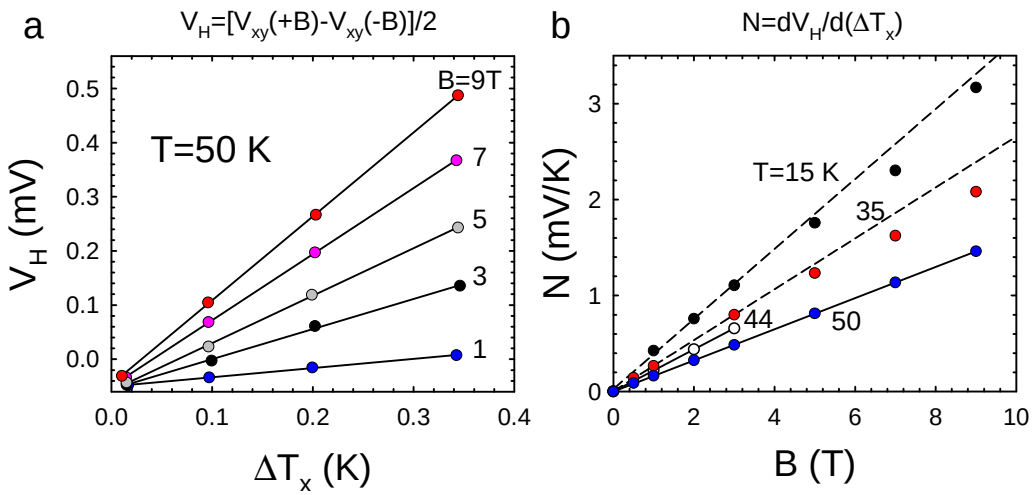

Fig. S 2: Variation of the Nernst voltage with longitudinal temperature difference at fixed fields (**a**) and field dependence of the Nernst signal at fixed temperatures (**b**).

The heat current in highly anisotropic crystals always has a small component along the nominally transverse direction during Nernst measurements. This induces a field-odd Nernst voltage across the *longitudinal* voltage leads. Thus, for an experiment with heat flow along b, ν_{bc} can be determined by extracting both the field-odd and field-even parts of V_{xx} and ΔT_y, respectively, the latter determined with an additional transverse thermocouple. This procedure yielded excellent agreement between values for ν_{cb} extracted from separate experiments on specimen C (discussed in Fig. 1) with heat currents $J_q||c$ and $J_q||b$. A field-odd component of ΔT_y produced by the Righi-Leduc effect was small, typically $< 10^{-2}\Delta T_x$, consistent with the small Hall angle.

Two-carrier analysis of magnetotransport

The magnetoresistance (MR) and Hall resistivity of a conductor with two carrier types and field-independent densities and mobilities can be expressed as[2, 3],

$$\Delta\rho(B)/\rho = \frac{MR_\infty(\mu_{eff}B)^2}{1+(\mu_{eff}B)^2} \qquad \text{and} \qquad \rho_H(B) = \frac{R_{H0}+R_{H\infty}(\mu_{eff}B)^2}{1+(\mu_{eff}B)^2}B$$

where,

$$MR_\infty = \frac{(\sigma^h R^h - \sigma^e R^e)^2}{\sigma^h\sigma^e(R^h+R^e)^2}, \qquad \mu_{eff} = \frac{\sigma^h\sigma^e(R^h+R^e)}{\sigma^h+\sigma^e}$$

$$R_{H0} = \frac{(\sigma^h)^2R^h+(\sigma^e)^2R^e}{(\sigma^h+\sigma^e)^2}, \qquad R_{H\infty} = \frac{R^hR^e}{R^h+R^e}$$

At $T > 50$ K the MR was quadratic and the Hall resistivity linear in field (Fig. S3), thus $R_{H\infty}$ is irrelevant. Simultaneously fitting the data at each temperature, with the additional condition that the measured zero-field

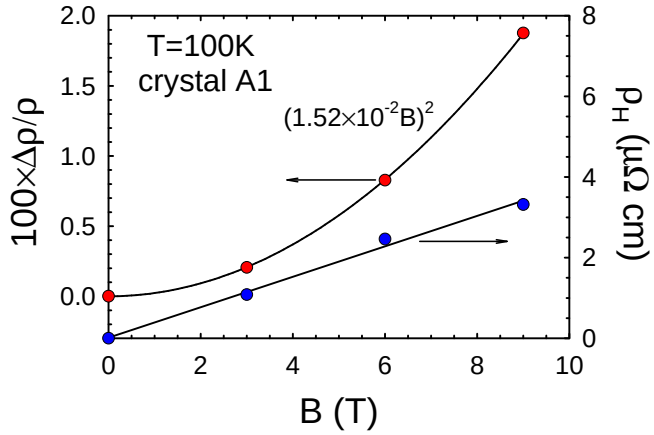

Fig. S 3: Magnetoresistance and Hall resistivity versus magnetic field for current applied along the conducting chains (b axis) and field along a.

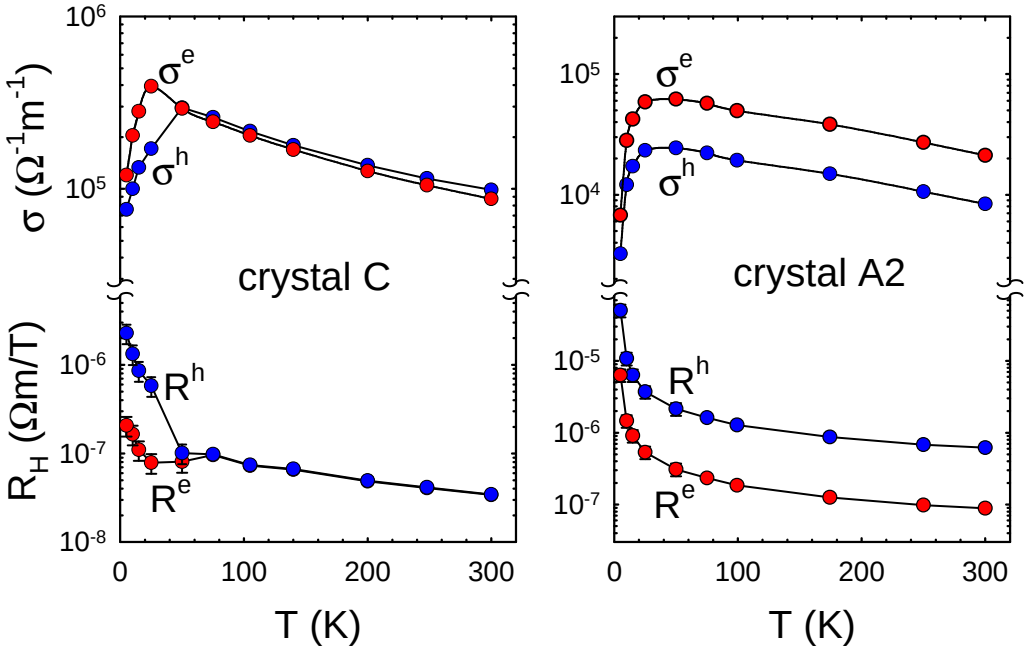

Fig. S 4: Hall coefficients and conductivities for holes and electrons along the conducting chains (b axis) from two-band model fitting. Error bars at $T \leq 50$ K reflect uncertainties associated with deviations of the MR from the two-band form (noted previously in Ref. 14).

conductivity be equal to $\sigma^h + \sigma^e$, highly constrains the four transport parameters. The reliability of parameter sets (determined using the Levenberg-Marquardt method) was established by varying the initial values of the parameters over a broad range. The results for crystals A2 and C are shown in Fig. S4.

Fermi temperature and mobilities

The Fermi temperature can be estimated from the energy difference between the Fermi level and bottoms of the two bands dispersing along the Γ-Y direction of the Brillouin zone, as determined by photoemission (0.25 and 0.49 eV, Ref. 8) or band structure calculations (0.38 eV and 0.62 eV, Ref. 9), i.e. $T_F \simeq (4-6) \times 10^3$ K. The dash-dot-dot curve labeled "$283\mu/T_F$" in Fig. 1 a uses $T_F = 5 \times 10^3$ K and $\mu = \mu^h + \mu^e$ computed as $\mu^i = \sigma^i R^i$ $(i = h, e)$ from Fig. S4.

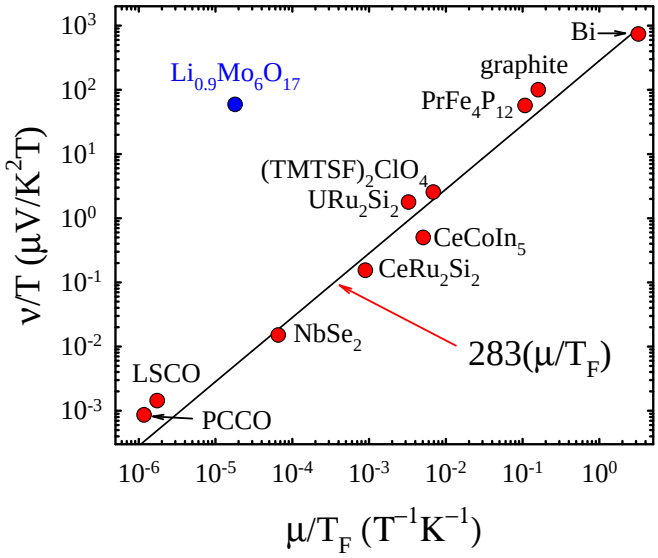

Fig. S 5: Low-T ν/T plotted versus μ/T_F for specimen C and a variety of other compounds (adapted from Ref. 5).

Estimate of Fermi temperature from the thermopower

Changes in the electronic structure at $T < T_m$ lead to a divergence of the TEP (Fig. 3) and thus preclude an estimate of T_F from the $T \to 0$ behavior of the diffusion thermopower. Instead we estimate T_F from the slopes of the linear-T thermopowers for specimens C, D, and E, under the assumption they reflect the diffusion contribution (we ignore the positive offsets in the TEP extrapolated to $T = 0$ for these specimens that are reminiscent of the TEP in cuprates [4]). The average value, $dS/dT = -0.045\mu\text{V/K}^2$, combined with the Mott expression under the assumption of a linear energy dependence of the conductivity at the Fermi level yields, $T_F = (\pi^2/3)(k_B/e)(-dS/dT)^{-1} \simeq 6.3 \times 10^3$ K. This agrees satisfactorily with the T_F estimates above given that the linear slope of our data should be smaller than those of either electrons or holes due to partial cancellation, $S = (\sigma^h S^h + \sigma^e S^e)/(\sigma^h + \sigma^e)$.

Carrier density estimated from chemistry/bonding

The two xy bands at E_F in the unit cell of $Li_{0.9}Mo_6O_{17}$ (composed of two formula units) are half full (Ref. 9), i.e. 1 electron per band or 2 mobile electrons per unit cell. The Li deficiency depletes charge (0.2 electrons per cell) from the chain Mo atoms, only half of which contribute to occupied orbitals at E_F. Thus the mobile charge per unit cell is estimated as $2 - 0.2/2 = 1.9$ electrons. With the unit cell volume, $V = 668$ Å^3, this yields $n = 2.84 \times 10^{27}$ m^{-3}. Oxygen deficiency should increase n from this value.

Seebeck coefficients computed from anisotropic Nernst expression

As noted in the text (Ref. 27), the Nernst coefficient for an anisotropic, bipolar conductor can be written as,

$$\nu_{yx} = \left(\frac{\sigma_x}{\sigma_y}\right) \frac{\sigma_x^h \nu_{yx}^h + \sigma_x^e \nu_{yx}^e}{\sigma_x} + \frac{(R^h \sigma_y^h - R^e \sigma_y^e)\sigma_x^h \sigma_x^e (S_x^h - S_x^e)}{\sigma_x \sigma_y} \tag{S1}$$

where $R^h(R^e)$ and $S^h(S^e)$ are the hole (electron) Hall and partial Seebeck coefficients, respectively, and $\sigma_x \equiv \sigma_x^h + \sigma_x^e$, etc. for σ_y. The Seebeck coefficient is defined as, $S_x = (\sigma_x^h S_x^h + \sigma_x^e S_x^e)/\sigma_x$. For perfect compensation, $\sigma_x^h = \sigma_x^e$, $\sigma_y^h = \sigma_y^e$, $R^h = -R^e$, the second term reduces to, $(1/2)\mu_x(S_x^h - S_x^e)$. Note that $\sigma_x^h = \sigma_x^e$ does not necessarily imply $\sigma_y^h = \sigma_y^e$. Since we have not measured the magnetoresistance for electric current along the c axis, for the calculations of S_b^h and S_b^e using eq. (S1) described in the text, we took $\sigma_c^h/\sigma_c = \gamma(\sigma_b^h/\sigma_b)$ with γ as an adjustable parameter. In addition to the case $\gamma = 1$ (shown in the inset of Fig. 3) we also show in Fig. S6 cases where holes are dominant for c-axis conduction ($\gamma = 1.8,\ 3$ for specimens A2, C) or electrons are dominant ($\gamma = 0.1$). Colossal Seebeck coefficients are found in either case.

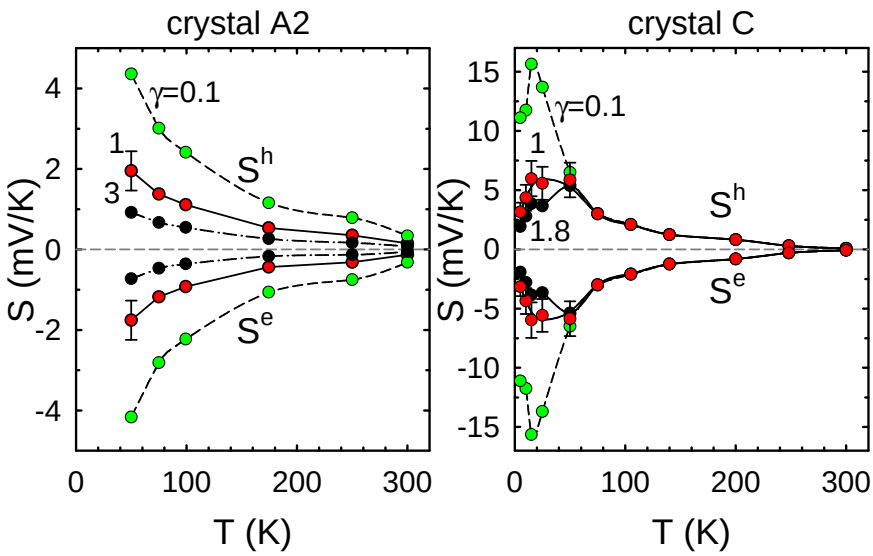

Fig. S 6: Hole and electron partial thermopowers computed using equation (S1) and the two-band thermopower expression, with the measured Nernst coefficients and two-band fit parameters from Fig. S4 as input. Error bars (25%) are propagated from Fig. S4.

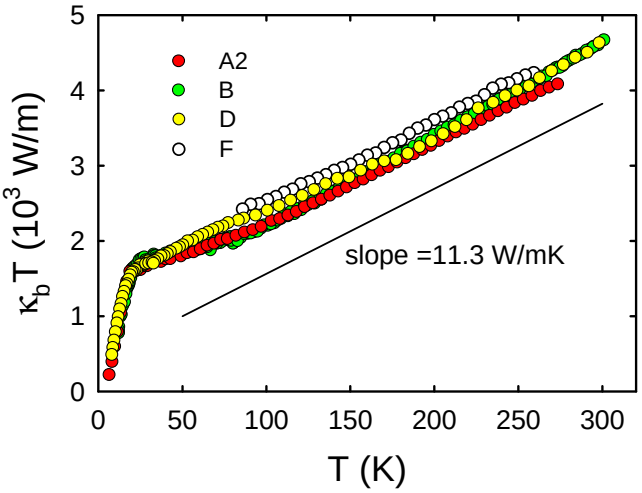

Fig. S 7: b-axis thermal conductivites, plotted as $\kappa_b T$ *vs.* T for four other crystals with σ_b(300 K) ranging from 0.8-3 mΩcm. Crystal F, not listed in Table I, had a c-axis lattice constant and thermopower very similar to that of specimen D.

[1] A. V. Inyushkin, K. Leicht, and P. Esquinazi, Cryogenics **38**, 299 (1998).
[2] A. B. Pippard, *Magnetoresistance in Metals,* Cambridge University Press, Cambridge, (1988).
[3] R. G. Chambers, Proc. Phys. Soc., London, Sect. A **65**, 903 (1952).
[4] S. D. Obertelli, J. R. Cooper, and J. L. Tallon, Phys. Rev. B **46**, 14928 (1992).